Structural Characterization of Mesoporous Organosilica Films for Ultralow-*k* Dielectrics

Femke K. de Theije,*,† A. Ruud Balkenende,† Marcel A. Verheijen,‡ Mikhail R. Baklanov,§ Konstantin P. Mogilnikov,§ and Yukiko Furukawa||

Philips Research Laboratories, Prof. Holstlaan 4 (WA11), 5656 AA Eindhoven, The Netherlands, Philips Centre for Industrial Technology, Prof. Holstlaan 4 (WY42), 5656 AA Eindhoven, The Netherlands, XPEQT at IMEC, Kapeldreef 75, B-3001 Leuven, Belgium, and Philips Research Leuven, Kapeldreef 75, B-3001 Leuven, Belgium

Received: December 12, 2002; In Final Form: February 27, 2003

A method to control the hydrophobicity and dielectric constant of mesoporous silica films for ultralow-*k* applications is described. Several surfactants have been used as sacrificial materials in (organo)silicate matrixes, prepared from tetraethoxysilane and methyltrimethoxysilane. To elucidate the relation between the composition of the films and their structure, the synthesis, chemical composition, mechanical properties, pore structure, crystallinity, and dielectric constant of the films were investigated. The high extent to which organic groups can be incorporated in these thin films opens the possibility to obtain a fully hydrophobic surface. Further, a combination of tetraethoxysilane and methyltrimethoxysilane leads to dense matrixes. The film properties were optimized for low-*k* applications by varying the processing conditions. Films containing 50−60% methyltrimethoxysilane in tetraethoxysilane and cetyl trimethylammonium bromide as a surfactant appear most attractive as a low-*k* material. These films are hydrophobic, have a dense matrix, and exhibit the smallest pore sizes (∼3 nm), which may facilitate integration issues.

1. Introduction

In the semiconductor industry, device features in integrated circuits (ICs) continue to shrink in order to increase the speed and the density of devices packed on the surface. Because of this shrinking, the increase in propagation delay, cross talk noise, and power dissipation of the interconnects become limiting factors in device performance.[1,2] To address resistance/capacitance delay,[3,4] copper wiring and low-*k* dielectrics are being developed to replace the Al/SiO_2 interconnect technology. Although a large variety of dielectric materials have been examined over the past years as low-*k* material, most candidates have been eliminated based on their inability to meet the integration criteria.[5] The transition from SiO_2, which has a dielectric constant of about 4, to new dielectric materials with $k < 3.0$ was delayed by about three years with respect to the initial semiconductor road map targets, because device integration proved more difficult than predicted.[2,6]

To lower the *k* values, a decrease in density and polarizability compared to SiO_2 is a prerequisite. Among potential candidates that have attracted a lot of attention in the recent past are porous organosilica materials.[7,8] In this study, we focus on porous organosilicates obtained by micelle templating. This method has the advantage that small, uniform pores can be combined with high porosities. Small pores are claimed to have a lower potential for cracking and delamination and thus ensure device structure integrity.[9] Furthermore, small pores facilitate integration issues (potentially less problems with sealing of the pores after etching and upon barrier deposition). These materials are also postulated to display higher mechanical strengths because of their engineered periodic structure.[10] In addition to a small pore size, prevention of water adsorption is crucial for obtaining a low dielectric constant.

This paper describes a method to control the structure, hydrophobicity, and dielectric constant of mesoporous hybrid inorganic−organic films for ultralow-*k* applications. In our approach, ionic as well as nonionic surfactants were used as sacrificial materials in (organo)silicate matrixes, prepared from tetraethoxy silane and methyltrimethoxysilane. Generally, the maximum amount of organically modified silicate that can be incorporated is about 40 mol %.[11] In this study, we report on the synthesis of ordered hybrid mesoporous films containing up to 90 mol % of methyltrimethoxysilane, whereby fully hydrophobic films can be prepared. To optimize the film properties and to attain insight into the structural aspects of the films in relation to their composition, several processing parameters, such as composition, surfactant type, and solution aging time were studied.

2. Experimental Section

Precursor solutions were prepared under acidic conditions in two steps. A typical starting mixture containing TEOS (tetraethoxy silane, $Si(OEt)_4$, yielding SiO_2 after curing), MTMS (methyltrimethoxy silane, $Si(OMe)_3CH_3$, yielding $SiO_{1.5}CH_3$, i.e., methylsilsesquioxane or MSQ), water, HCl, and ethanol was heated at 60 °C for 90 min. The amount of MTMS versus TEOS was varied from 0 to 100 mol %. A total of 0.25 mol of water were added per alkoxy group, and ethanol and HCl were added in molar ratios of 3 and 5×10^{-5} relative to the silicate precursors, respectively. Under these conditions, the silicates are partly hydrolyzed, while preventing significant condensation. This mixture was then diluted with ethanol. Additional water,

* To whom correspondence should be addressed. E-mail: femke.de.theije@philips.com. Phone: +31 40 2742577. Fax: +31 40 2744282.
† Philips Research Laboratories.
‡ Philips Centre for Industrial Technology.
§ XPEQT at IMEC.
|| Philips Research Leuven.

10.1021/jp027701y CCC: $25.00
Published on Web 04/11/2003

HCl, and the surfactant were added. The solutions were typically used after 3 days of aging. Various surfactants, like the ionic cetyl trimethylammonium bromide (CTAB, $C_{16}H_{33} - N(CH_3)_3^+ Br^-$), and several nonionic surfactants, including Brij76 ($C_{18}H_{37}(OCH_2CH_2)_{10}OH$) and Pluronic F127, have been used. The Pluronics are poly(ethylene oxide)−poly(propylene oxide)−poly(ethylene oxide) triblock copolymers, and the molecular formula for F127 is $PEO_{106}-PPO_{70}-PEO_{106}$. This surfactant forms a mesophase under acidic conditions, because the PEO block is more hydrophilic than the PPO block. The final mole ratios in the case of CTAB were typically: silicate:ethanol:H_2O:HCl:CTAB = $1:20:5:4 \times 10^{-3}:0.08-0.30$. For the other surfactants, equivalent volumes are used.

Variations in this preparation procedure were examined. MTMS was replaced by DMDES (dimethyl diethoxysilane, $Si(OMe)_2(CH_3)_2$). These films gave similar properties (porosities and dielectric constants) if the total amount of CH_3 groups was kept the same (i.e., the molar ratio of DMDES is $^1/_2$ times that of MTMS).

To prepare mesoporous thin films, a sol−gel solution containing surfactants was spin-coated onto a silicon (001) substrate. After deposition, the coatings were dried for 2 min at 130 °C on a hot plate. Subsequent annealing was usually performed for 30−60 min at 400 °C in air, leading to the further condensation of the silicate matrix and the removal of the surfactant. The film thickness ranged from less than 100 nm up to 1.7 μm, dependent on the spin speeds (varied between 750 and 2000 rpm) and the extent of dilution of the coating solution with ethanol (the molar ratio of silicate:ethanol was varied between 1:10 and 1:30). Unless indicated otherwise, all experimental results are obtained after annealing of the film.

Ellipsometry, Fourier transform infrared spectroscopy (FTIR), small angle $\theta-2\theta$ X-ray diffraction (XRD), atomic force microscopy (AFM, DI Nanoscope III), scanning electron microscopy (SEM, Philips XL30), and transmission electron microscopy (TEM, Philips CM30ST and TECNAI F30ST) were used for the structural and optical analysis of the films. The mechanical properties were studied by stress measurements (Tencor FLX 2900) and measurements of the Young's modulus (E). To determine E, three techniques are used: nanoindentation (NI), surface acoustic wave spectroscopy (SAWS), and ellipsometric porosimetry (EP). NI measurements are performed using a Nanoindenter from MTS with Dynamic Contact Module, utilizing a Continuous Stiffness Measurement. In these measurements, a small oscillation (~1 nm) is superimposed on the overall linear increase of the diamond tip's (Berkovich) contact depth. The dynamic response yields a harmonic contact stiffness that can be used to calculate a modulus depth profile. However, because of the spatial extent of the elastic deformation field, the presence of the hard substrate will almost immediately result in an increasing value only partly related to the film properties. An accurate determination of the moment that surface contact is made to within 2 nm is critically important for the determination of E from nanoindentation on these thin low modulus layers ($E < 10$ GPa). Typically, simultaneously monitoring the load on the sample, the harmonic contact stiffness, and the phase angle between applied oscillation and resulting tip displacement gives sufficient information even in the presence of a thin adsorbant layer. The two other techniques to evaluate E are surface acoustic wave spectroscopy (SAWS)[12,13] and EP.[14] The surface acoustic wave packet propagates in both layer and substrate. Waves of different frequency sample a different proportion of layer and substrate, with different net elastic properties. The wave velocity is therefore frequency dependent, and the wave packet becomes dispersed. The shape of the dispersion curve is characteristic of the elastic properties of the layer−substrate system. To calculate E from EP measurements, the film shrinkage because of capillary condensation is monitored as a function of the relative toluene pressure. This shrinkage is an elastic response to capillary forces that depend on the elastic properties of the film and can be used to calculate the E of thin porous films. The dielectric constant (ϵ') of the films was determined using an impedance analyzer operating at 1 MHz using highly conductive Si as the substrate (ρ = 0.001−0.005 Ωcm) and the double contacts of a mercury probe (MSI Hg 612) as electrodes. The porosity was calculated from the refractive index (n), obtained from ellipsometry using the Bruggeman effective medium approximation,[15] assuming the refractive index of the matrix to be 1.46 (which is the refractive index of fused SiO_2). This assumption was supported by analysis of ellipsometric porosimetry (EP) data (see section 3.3). The pore sizes were assessed from TEM, XRD, and 2 adsorption−desorption techniques, EP and krypton adsorption. EP uses toluene as the adsorbate and combines adsorption porosimetry with ellipsometry to measure pore sizes, pore size distributions, and refractive indices of the matrix of porous films. The amount of adsorbate is measured as a function of the relative vapor pressure by ellipsometry from the measured change of optical characteristics of the porous film during a vapor adsorption/desorption cycle. Measurements are carried out at room temperature; the adsorbate should be a volatile liquid, because of the need to work near the equilibrium pressure P_0. Kr adsorption uses krypton as the adsorbate and uses the volumetric measurement of adsorbed amounts during an adsorption/desorption cycle. Measurements are carried out at liquid-nitrogen temperatures. Krypton was chosen over nitrogen adsorption, because the equilibrium vapor pressure of Kr at liquid-nitrogen temperature is much lower than that of N_2 (2.49 mbar for Kr versus 1 bar for N_2). Therefore, by using Kr adsorption, the detection sensitivity is improved so that also samples with small absolute surface areas, such as thin porous films, can be measured accurately.

3. Results and Discussion

3.1. Surfactants: Ionic versus Nonionic. In a previous paper,[16] we showed that the maximum amount of CTAB, an ionic surfactant that can be added to TEOS-based films without collapse of the pore structure upon annealing, is dependent on the amount of methyl groups in the film. For TEOS-based films, the maximum porosity that can be obtained was 45%, whereas for layers obtained from MTMS−TEOS mixtures, porosities of up to 60% could be obtained. The lower maximum porosity of TEOS-based films is assumed to be due to the close vicinity of reactive hydroxyl groups inside the small pores, leading to slow further condensation of the network and thereby collapse of the pores. However, if the nonionic Pluronic F127 is used as a surfactant, TEOS-based films can attain much higher porosities without pore collapse (Figure 1). For Pluronic F127 films, the pores that are formed are about 3 times larger compared to those of CTAB films (see section 3.3). Although this makes the films less attractive for use as a low-k material, it is easier to obtain higher porosities. Furthermore, for a nonionic surfactant like F127, the walls between the pores generally are thicker (for mesoporous silica prepared under acidic conditions a wall thickness of 3.8 nm is mentioned for nonionic surfactants,[17] whereas for ionic surfactants a wall thickness of 1.0−1.5 nm is reported[18,19]). In combinition with the smaller radius of curvature, this explains the stability of F127 containing TEOS-based

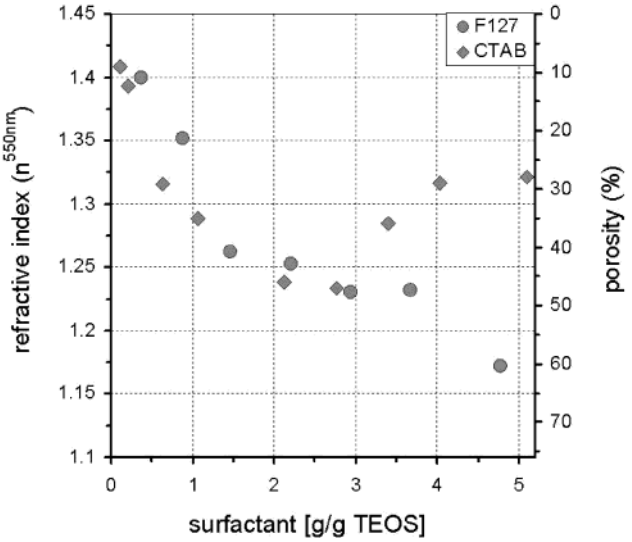

Figure 1. Refractive index, measured in dry N_2 atmosphere, and the corresponding porosity of TEOS-based films as a function of surfactant content during preparation. Values are measured after annealing at 400 °C.

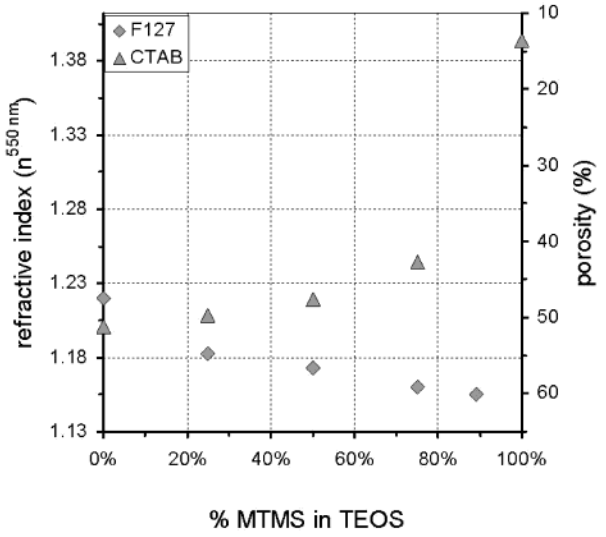

Figure 2. Refractive index and porosity of thin films prepared with either 10 mol % CTAB or 0.5 mol % F127 as a surfactant, measured after annealing at 400 °C. The ratio of MTMS-to-TEOS is varied.

films over time. Even highly porous films do not collapse, and the porosity remains high. The porosity and refractive index of TEOS-based films as a function of surfactant concentration, for CTAB as well as F127, are shown in Figure 1.

The difference in collapse behavior of films prepared from the two surfactants is also clear when the composition of the matrix is varied, whereby the molar ratio of surfactant is kept constant. Films prepared from different MTMS/TEOS ratios and from 10 mol % CTAB (i.e., below the concentration for which collapse of TEOS films is observed) show a decrease in porosity with increasing amount of methyl groups. The effect of an increasing methyl content is opposite for F127-based films, as is shown in Figure 2. This can be caused by the smaller wall thickness for CTAB-based films compared to those for F127-based films. For the CTAB films with a small wall thickness (1−1.5 nm, less than 10 atoms), an increase of the amount of methyl groups reduces the rigidity by reducing the degree of cross-linking to a level too small to retain the structure after surfactant removal. On the other hand, increasing the amount

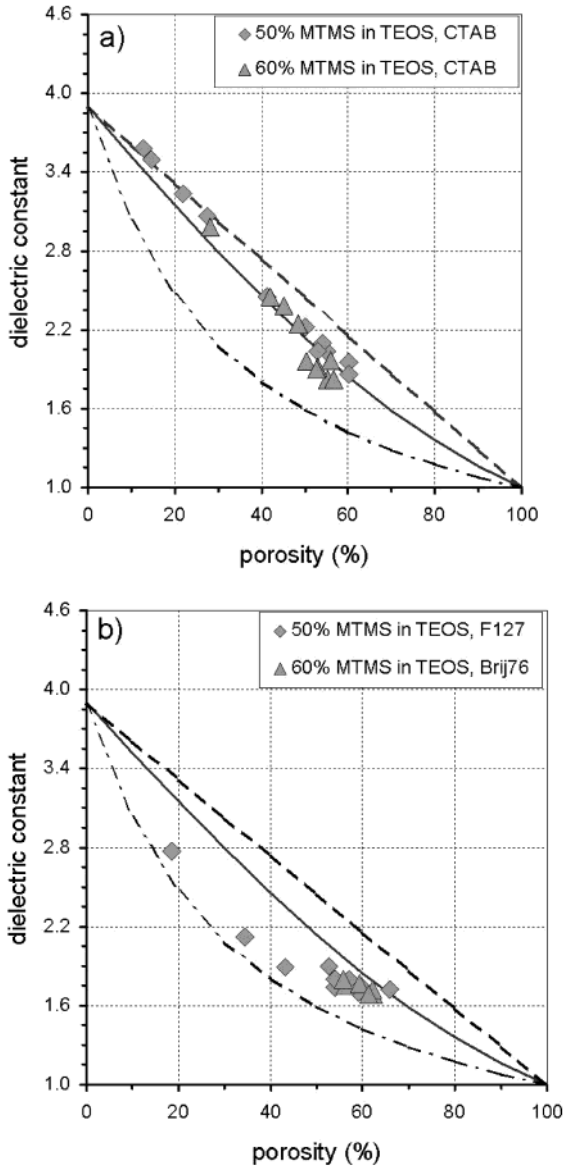

Figure 3. Dielectric constants (at 1 MHz) as a function of the porosity for mesoporous layers prepared from varying MTMS-to-TEOS ratios and (a) CTAB as the surfactant and (b) various nonionic surfactants. The solid curve represents calculated values using the dielectric constant of dense SiO_2 and the Bruggeman effective medium approximation, and the dashed-dotted curve represents a layer or series model and the dashed line represents a parallel model.

of MTMS leads to a more elastic film (see section 3.4). Hereby the contraction of the layer upon annealing of the films is reduced. For F127-based films, having thicker walls and thus less problems retaining rigidity upon loss of the degree of cross-linking leads to higher porosities. Further, the interaction between the silicate and the surfactant will be different for an ionic and nonionic surfactant, which may also influence the stability of the films.

The dielectric constant of films prepared from ionic or nonionic surfactants also shows differences as a function of porosity. Figure 3a shows the results for hydrophobic layers with CTAB as the surfactant, measured in dry nitrogen, after exposure to ambient air. The data follow the Bruggeman approximation quite nicely. These results show that a higher content of the less polarizable methyl groups results, as expected, in smaller values for the dielectric constant. For CTAB, the large amount of surfactant that can only be used in combination with a high MTMS content, leads to values for ϵ' as low as 1.8. On

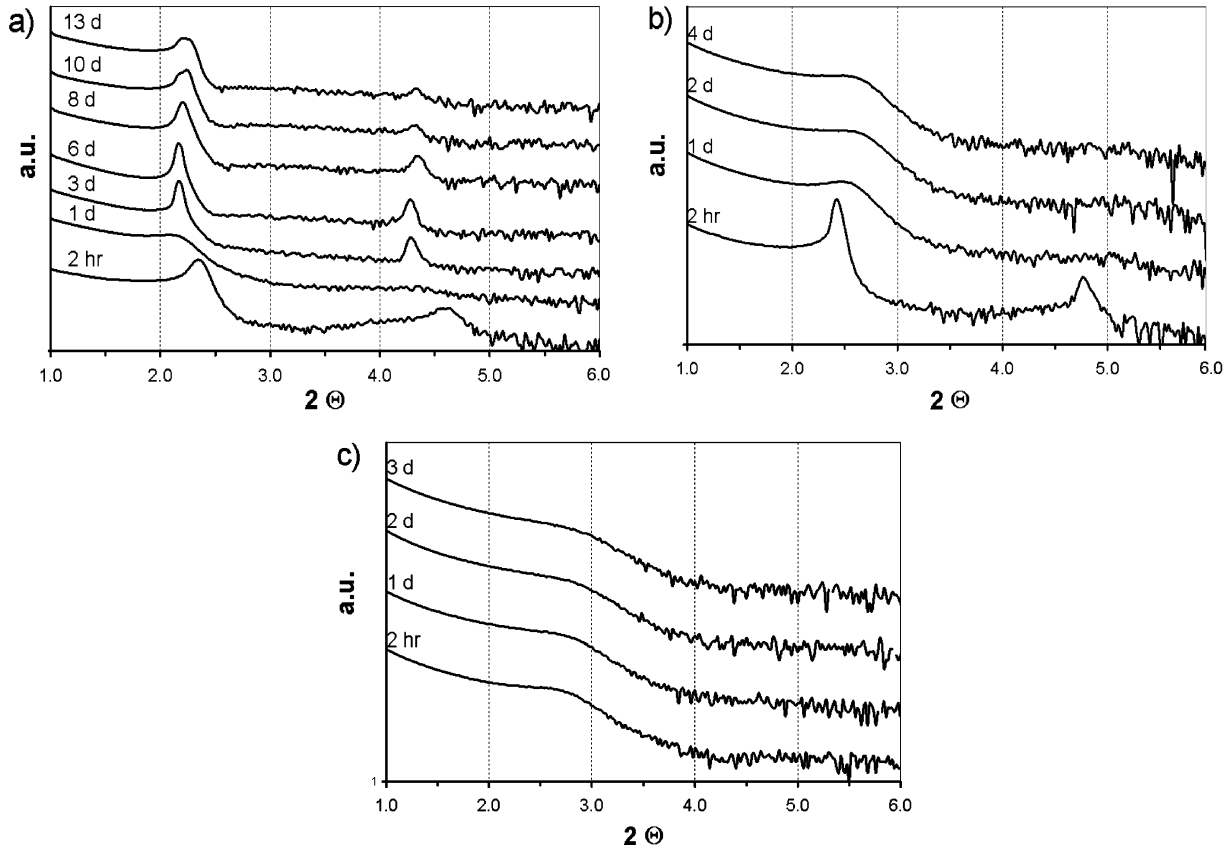

Figure 4. $\theta-2\theta$ X-ray diffraction spectra for annealed films prepared with CTAB as the surfactant in a molar ratio of 10 mol % (a) TEOS-based films (b) 33% MTMS in TEOS-based films, and (c) 50% MTMS in TEOS-based films. The aging times vary.

the other hand, if nonionic surfactants are used, higher porosities can be obtained, which is related to the larger pores. Therefore, the minimum dielectric constant for the films based on nonionic surfactants is lower and can be as small as 1.7. The results are presented in Figure 3b. Especially for the lower porosities, the dielectric constants are much lower than expected from the Bruggeman approximation (which is valid for interconnected spherical inclusions). This implies that this model is not valid for the type of voids generally observed with nonionic surfactants, i.e., cylindrically shaped pores, which are lying parallel to the substrate. For low porosities, the dielectric constants found for these films are closer to a stacked layer model, in which the different capacitors (matrix and air) are connected in series.

3.2. Pore Structure. *Pore Periodicity from Small-Angle X-ray Diffraction.* Surfactant-templated films have small and uniform pores and exhibit an ordered pore structure. This pore ordering can be observed by small-angle X-ray diffraction. A series of XRD patterns for mesoporous coatings with 10 mol % CTAB as the surfactant and 0−75% MTMS in TEOS has been measured.[16] From 2D XRD measurements,[20] it was concluded that before annealing these layers exhibit a 3D-hexagonal pore ordering with the *c* axis perpendicular to the substrate surface. Annealing induces shrinkage in the *z* direction of the films. Hereby the *d* spacing and film thickness reduce by 15−25%, and the hexagonal pore ordering is contracted. TEM images (Figure 5) show that the pore structure after annealing corresponds to a slightly distorted rectangular or cubic structure. The *d* spacing found from XRD gives information about the interpore distances. For these pore systems, the interpore distance is close to $\sqrt{2}\ d_{(001)}$. The interpore distance decreases with increasing methyl content as given in Table 1. With increasing methyl content, the intensity of the Bragg reflection decreases, indicating a significant loss of long-range mesoporous ordering compared to the pure silica case. The loss in pore ordering that was observed with XRD does not indicate a loss of mesoporosity, as was checked by ellipsometric porosimetry. Films prepared from solutions containing 10 mol % CTAB and varying amounts of methyl groups all showed a small pore size distribution. The diameter of the pores measured by EP was 2.3 nm for a 50% MTMS in TEOS film, for 75% MTMS in TEOS 2.7 nm was found, and for 90% MTMS in TEOS the pore diameter was 2.5 nm.

The pore ordering further depends on the aging time of the solution. For TEOS-based films, the optimum aging time is 3−6 days (see Figure 4). With increasing MTMS content, the optimum aging time decreases to 2 h for a solution containing 33% MTMS in TEOS (see Figure 4b). For higher MTMS contents (50% or more, see Figure 4c), the long-range ordering is weak and does not significantly change over time.

Pore Periodicity as Measured by TEM. For a well-ordered film, a cross section or top view TEM image can be used to measure the periodicity of the pores directly. The pore ordering is sufficient to obtain measurable values for films containing at most 33% MTMS in TEOS, samples with MTMS contents above 33% cannot be measured. A number of samples containing CTAB or F127 as surfactant were studied. A film prepared from 33% MTMS in TEOS with CTAB as the surfactant shows pore periodicity perpendicular to the substrate of 2.8 nm before the annealing step and 2.7 nm after annealing. For annealed TEOS-based films prepared from F127 as the surfactant, values of 6.5 to 7.8 nm are found perpendicular to the surface, and parallel to the surface, these values vary between 6.6 and 8.0 nm. It should be noted that it cannot be excluded that the preparation of the cross sections (mechanically polishing or focused ion beam) induces a variation in the measured periodicity. Only the top-view images (see Figure 5a) obtained from

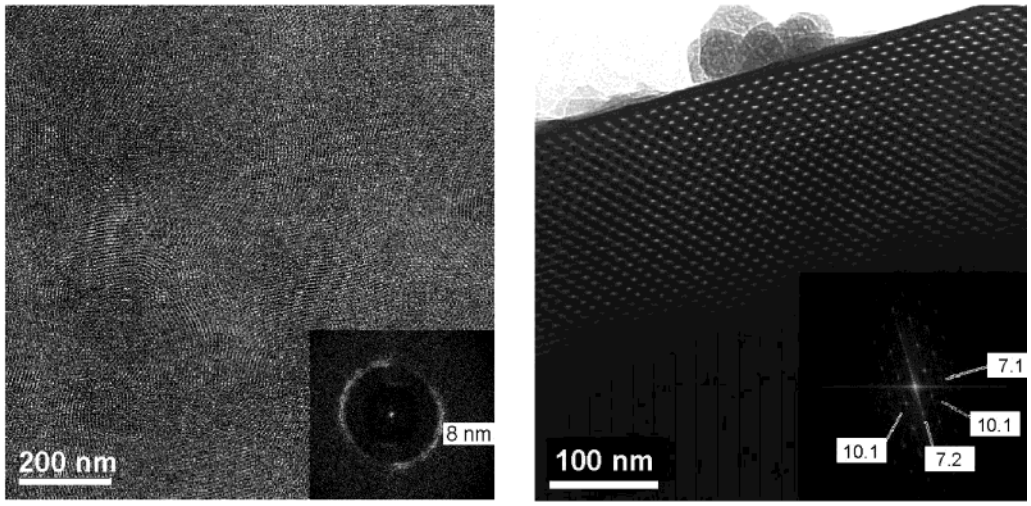

Figure 5. (a) Top view and (b) cross section of a TEOS-based film prepared from 0.5mol % F127 as the surfactant. The inset in part a gives the Fourier transform of the image, showing the in-plane isotropy and the periodicity of 8 nm. The inset in part b gives the Fourier transform of the cross section, showing a cubic pore structure with $a = b = 10.1$ nm.

TABLE 1: *d* spacing and Interpore Distance for Annealed Films as a Function of the MTMS Content in a Film Prepared from Solutions Containing 10 mol % CTAB and Assuming a Cubic Pore System

% MTMS in TEOS	d-spacing (nm)	interpore distance (nm)
0%	3.4	4.8
25%	3.2	4.5
50%	2.8	3.9
75%	2.5	3.5

films deposited on a TEM window[21] do not have any TEM preparation step.

Pore Sizes as Measured by Adsorption−Desorption Techniques. Two adsorption−desorption techniques have been used to measure the pore sizes of our dielectric films: krypton adsorption and ellipsometric porosimetry (EP). For mesopores (>2 nm), the pore size distribution is calculated from the desorption isotherm assuming desorption from cylindrical pores. The Kelvin equation then gives

$$r_k = \frac{2\gamma V_l \cos\theta}{RT \ln(p/p_0)} \quad (1)$$

where γ is the surface tension, $V_l$is the molar volume of the adsorbate, θ is the contact angle of the adsorbate (which is taken to be 0), R is the gas constant, T is the measurement temperature, p/p_0 is the relative pressure, and r_k is the Kelvin radius. The radius of the pore is then $r_p = r_k + t$, in which t is the thickness of the adsorbed layer before capillary condensation occurs. This thickness t is obtained from the data for the adsorption of the same adsorptive on a nonporous sample having a similar surface. For micropores (<2 nm), the Dubinin−Radushkevich (DR) analysis is used.[22] This model is based on a thermodynamic description of micropore filling. Figure 6 shows the adsorption and desorption isotherms and the corresponding pore size distribution for a film prepared from 50% MTMS in TEOS and 7.6 mol % CTAB. The pore diameter as measured with EP is about 2.0 nm.

The same type of samples that were measured by EP were also measured by Kr adsorption. The problem that is encountered for toluene adsorption also occurs for Kr adsorption: the calculated pore size is determined by the model one uses (DR or Kelvin; shape of the pores: spherical, cylindrical, or lamellar). Furthermore, for Kr adsorption, it cannot be defined based on

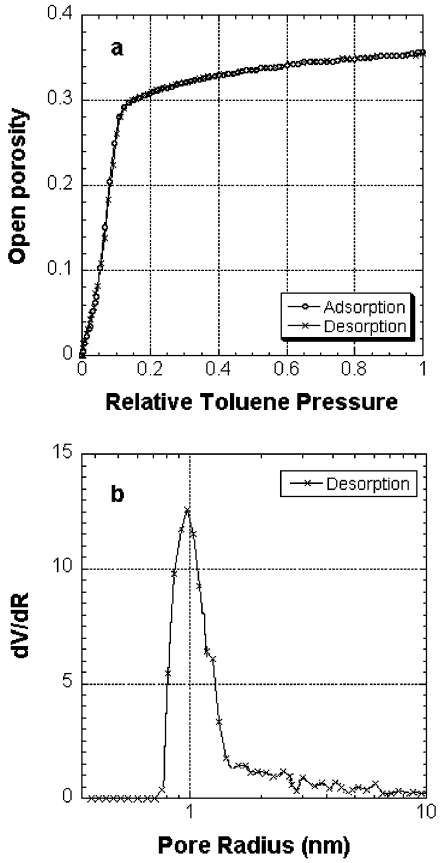

Figure 6. Toluene adsorption−desorption isotherm (a) and pore size distribution (b) for a film prepared from 50% MTMS in TEOS and 7.6 mol % CTAB as a surfactant.

the shape of the sorption isotherm if the confined fluid phase is a solid or a liquid. This means that it is not clear which values for the saturation pressure, surface tension, and density should be used for the pore size calculation. We used the data presented in ref 23 to calculate the pore size. Figure 7 gives the results for the series of films prepared from solutions containing 50% MTMS in TEOS and varying amounts of CTAB, measured by EP as well as by Kr adsorption.

The increase of the pore size measured with Kr adsorption as well as with EP with increasing amounts of CTAB is remarkable and in apparent contradiction with the *d* spacing as

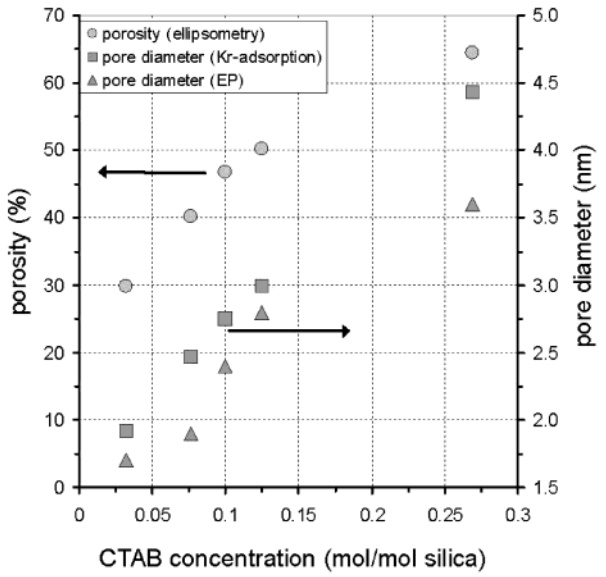

Figure 7. Porosities (measured by ellipsometry) and pore sizes (as measured by Kr adsorption and EP) of films prepared from solutions containing 50% MTMS in TEOS and varying amounts of CTAB.

TABLE 2: *d* spacings, Interpore Distances (based on a Cubic Pore Systems where This Distance Equals $\sqrt{2}\ d_{(001)}$), and Pore Sizes (based on an Average of the Values Found by EP and KR Adsorption) of Films Prepared from Solutions Containing 50% MTMS in TEOS and Varying Amounts of CTAB

CTAB amount	d-spacing (nm)	interpore distance (nm)	pore size (nm)
7.6 mol %	2.8	3.9	2.2
10 mol %	2.7	3.8	2.6
12.5 mol %	2.6	3.6	2.9
26.9 mol %	2.2	3.1/2.2 [a]	4.0/2.0 [a]

[a] For a lamellar system.[24]

measured by XRD, which decreases for increasing CTAB concentrations (see Table 2). Partly, this may be due to a decrease in wall thickness with higher CTAB concentrations. For concentrations less than 8 mol %, the small pore size is explained by the fact that in these films the critical micelle concentration is not reached, so that micelles are not formed. At higher CTAB concentrations, the pore size is seen to increase almost in proportion to the porosity, which points to an increasing micelle size. This might be due to a transition from spherical to cylindrical pores. For the highest CTAB concentrations, however, the interpore distance (measured based on cubic pore systems where this distance equals $\sqrt{2}\ d_{(001)}$) is smaller than the measured pore size. Therefore, it is speculated that this disagreement is due to a change in the pore shape. It is well-known that at very high CTAB concentrations usually a lamellar phase is favored. Although a really lamellar phase would collapse upon surfactant removal, it can be envisaged that platelike pores are formed. In that case, the pore size as calculated would be overestimated by about a factor of 2,[24] as the shape of the meniscus from which desorption takes place would change from double curved to single curved.

Also the pore diameters of films containing different surfactants were measured by EP, and the results are given in Table 3. It is clear that CTAB gives by far the smallest pores, which is attractive for low-*k* applications. In Table 3 also, the refractive index calculated for the matrix of the material is given. This refractive index is close to the 1.46 of fused SiO_2. Usually, MTMS-containing films exhibit a smaller value of the refractive

TABLE 3: Porosities (Measured by Ellipsometry), Average Pore Sizes, Matrix Densities (Measured by EP), and Dielectric Constants (Measured at 1 MHz) of Films Prepared from Solutions Containing 50% MTMS in TEOS and Varying Surfactants

surfactant	porosity	average pore diameter (nm)	refractive index of the matrix	dielectric constant @ 1 MHz
16 mol % CTAB	56%	3.0	1.46	2.0
14 mol % Brij76	62%	6.5	1.43	1.7
0.65 mol % F127	60%	8.0	1.46	1.8

index in the range of 1.38 to 1.40. However, such films have a relatively low density. The high refractive index therefore points to a high density of the wall material. In agreement with this observation is the absence of micropores in the present films, whereas micropores of about 1 nm are observed (with ellipsometric porosimetry) in mesoporous methyl silsesquioxane films.

Comparison of the Different Techniques Used to Measure Pore Sizes. It is clear that all techniques to measure pore sizes have their own disadvantages. XRD and TEM measure periodicities, to obtain interpore distances the "crystal" structure of the pores must be known, whereas the wall thickness of the matrix material should be known to determine pore sizes. Furthermore, XRD gives an average over the film, whereas TEM is a local technique that is only suitable for well-ordered films (not applicable for a MTMS ratio exceeding 33%). In addition, deviations can be introduced by the preparation of the film before observation. EP and Kr adsorption are indirect techniques: an idealized model of the pore shape, which uses partly uncertain material properties of the adsorbate and the porous material, is used to calculate the pore sizes. Therefore, the pore diameters obtained from the different techniques vary considerably. The pore sizes measured by EP are somewhat lower than those measured by Kr adsorption. Furthermore, the *d* spacings (XRD) decrease, whereas the pore sizes increase with increasing CTAB content. Partly, this will be due to a decrease in the wall thickness of the pores for higher CTAB concentrations but also a structural rearrangement in the ordering of the pores with changing surfactant concentration might play a role.

3.3. Matrix Material. *Chemical Composition.* To investigate the effect of a variation in the chemical composition, a series of films is deposited on Si wafers with varying MTMS/TEOS ratios and a constant surfactant ratio of 10 mol % CTAB relative to Si. The changes in chemical composition of films with varying methyl (MTMS) content are followed by FTIR. The transmission spectra, collected in air, are shown in Figure 8a. For all of the spectra presented, the transmission spectrum of the Si substrate was subtracted.

The Si−O−Si antisymmetric stretching modes appear as discrete bands centered at about 1050 and 1130 cm^{-1}.[25] With increasing organic content, a shift of the main Si−O−Si vibration from 1075 to 1042 cm^{-1} is observed, indicating that the Si−O−Si framework is loosened by the substitution of Si−CH_3 for Si−O−Si.[26] This shift shows that the degree of cross-linking of the silica network changes if methyl groups are added to the system. Further, the height of peaks due to methyl (CH_3 stretch at 2977 cm^{-1}, CH_3 deformation at 1278 cm^{-1}, and Si−CH_3 at 778 cm^{-1} [27]) gradually increases with increasing methyl content.

The bands due to hydroxyl vibrations decrease with increasing methyl contents. The peak at 945 cm^{-1}, which is indicative for the presence of silanol peaks, is clearly visible for the TEOS film, decreases for the 25% MTMS film, and is not present for the higher methyl contents. Coupled to this, the amount of water

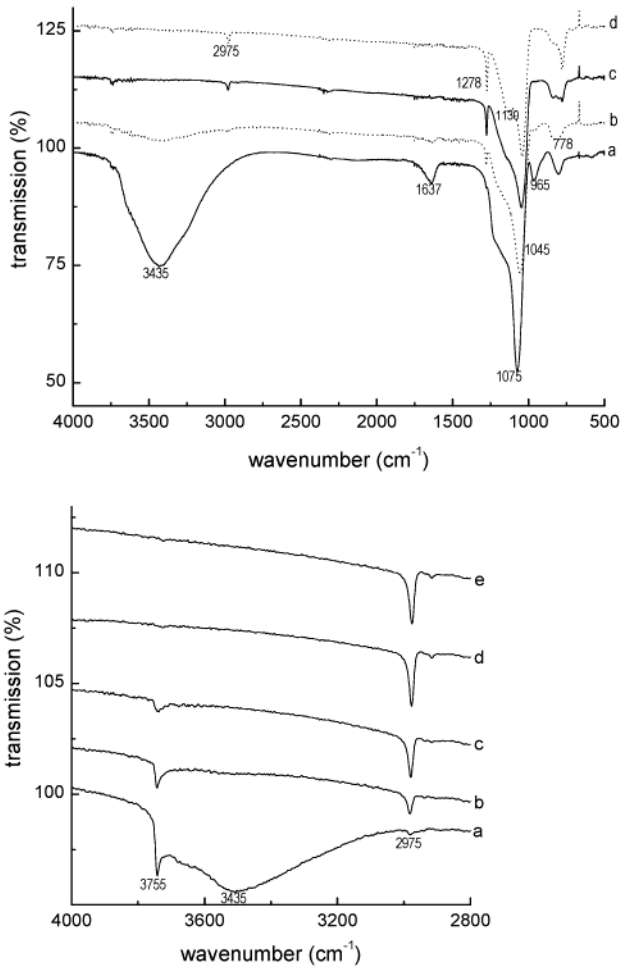

Figure 8. FTIR transmission spectra, measured in air (left) and in dry nitrogen (right), of mesoporous films prepared with 10 mol % CTAB and various amounts of MTMS and TEOS. The molar ratios of MTMS to total silica for the different curves are (a) 0%, (b) 25%, (c) 50%, (d) 75%, and (e) 90%. The curves have been shifted for clarity.

adsorbed in the pores decreases with increasing methyl content. The OH-stretch and OH-bend vibrations, at 1637 and around 3300−3700 cm^{-1}, show the same trend as the Si−OH peak at 945 cm^{-1}. Only a small peak at 3600 cm^{-1} due to isolated hydroxyl groups remains for films with a high methyl content. This is an important observation if the material is to be used as a low-*k* film. The absence of water in films prepared from at least 50% MTMS induces a lower dielectric constant ($\epsilon'_{water} = 78.5$). Furthermore, low-*k* back-end integration problems such as via poisoning and delamination caused by water in the films can be avoided.

To avoid the large water signals in the IR spectra, FTIR spectra were also measured in dry nitrogen and are given in Figure 8b. In the TEOS-based film, a broad and complex band centered around 3435 cm^{-1} dominates the IR spectrum in the O−H stretching region. This band is due to the interaction of water molecules via hydrogen bonds with Si−OH groups inside the pores. The other samples, which contain less or no Si−OH groups (as evident from the Si−OH peak at 3755 cm^{-1}) show no presence of adsorbed water. Furthermore, the CH_3 stretch at 2975 cm^{-1} increases with increasing methyl content.

Crystallinity. With the exception of ordered hexagonal mesoporous benzene−silica materials with bridging organic groups,[28] crystallinity of the matrix material of ordered mesoporous silica films has not been reported.[29] However, TEM results showed (partial) crystallinity in the matrix material of annealed films, whereas no crystallinity was observed for as-prepared films. The presence of surfactant seems to be a necessary requisite: in films prepared without surfactant, crystallinity has not been observed. Generally, only a few percent of the film is observed to be crystalline. No evidence for the simultaneous local occurrence of pore ordering and atomic-scale ordering has been found in our TEM results, although this cannot be excluded on the basis of the present results. However, the relative ease of crystallization indicates that the matrix material is dense, which can be an advantage for integration issues (the absence of microporosity is expected to facilitate sealing of the pore walls after etching). Crystallinity has been observed in films containing 0−50% MTMS in TEOS and for films prepared from both ionic as well as nonionic surfactants. Figure 9 shows some examples of crystalline regions in cross sections mechanically polished to electron transparency. Figure 9a shows a part of a film prepared from a solution containing 33% MTMS in TEOS and 10 mol % CTAB. This piece is polycrystalline, with crystals of 50−100 nm in size. Electron diffraction of this cross section resulted in a set of interplanar distances d_{hkl} varying from 0.94 to 2.31 Å. Figure 9b shows a high-resolution TEM image of the cross-section of a film based on a solution containing 50% MTMS in TEOS and a CTAB concentration of 10 mol %, and the interplanar distance is 3.11 Å. In Figure 9c, a high-resolution cross section of a film prepared from pure TEOS and a F127 concentration of 0.5 mol % is shown. The Fourier transform of this image resulted in interplanar distances of 2.08, 2.22, and 2.84 Å.

It is difficult to deduce the mechanism of crystallization for mesoporous organosilica films. The preparation technique might play a role in the crystallization of the matrix material. On the other hand, the mechanical forces are not that severe that one would expect crystallization just by applying force to the film. The hypothesis that MTMS facilitates crystallization and is therefore a necessary condition, which was posed because crystallization in mesoporous has never been reported for TEOS-based films, although they are studied frequently,[30,31] does not hold because in one TEOS-based sample crystallization was also observed (Figure 9c). Up to now, crystallinity was only found in mesoporous films, not in dense films, so surfactant templating might induce the crystallization. The crystal structure of the organosilica matrix cannot be deduced from the limited set of TEM-based interplanar distances because no crystal structures are known for silica structures containing methyl groups. Furthermore, in XRD, crystallinity could not be observed, and high resolution TEM and electron diffraction provide a lot of different interplanar distances, which also generally vary for different films.

3.4. Mechanical Properties of the Films. *Tensile Stresses Induced by the Films.* The stress in the film after deposition should be very small for low-*k* applications. Stress may cause fracture within the film or adhesion failure between film and substrate. Further, stress causes curvature of the substrate; stresses above 50−100 MPa complicate the handling of wafers using a vacuum chuck. The stress on films deposited onto a substrate can be obtained by measuring the radius of curvature of a substrate wafer before and after deposition of a film. The relation between the radius of curvature and the stress in the film is given by

$$\sigma = \frac{Eh^2}{(1-\nu)6Rt} \qquad (2)$$

whereby σ is the stress in the thin film, $E/(1-\nu)$ the biaxial elasticity modulus of the substrate (E is the elastic modulus and

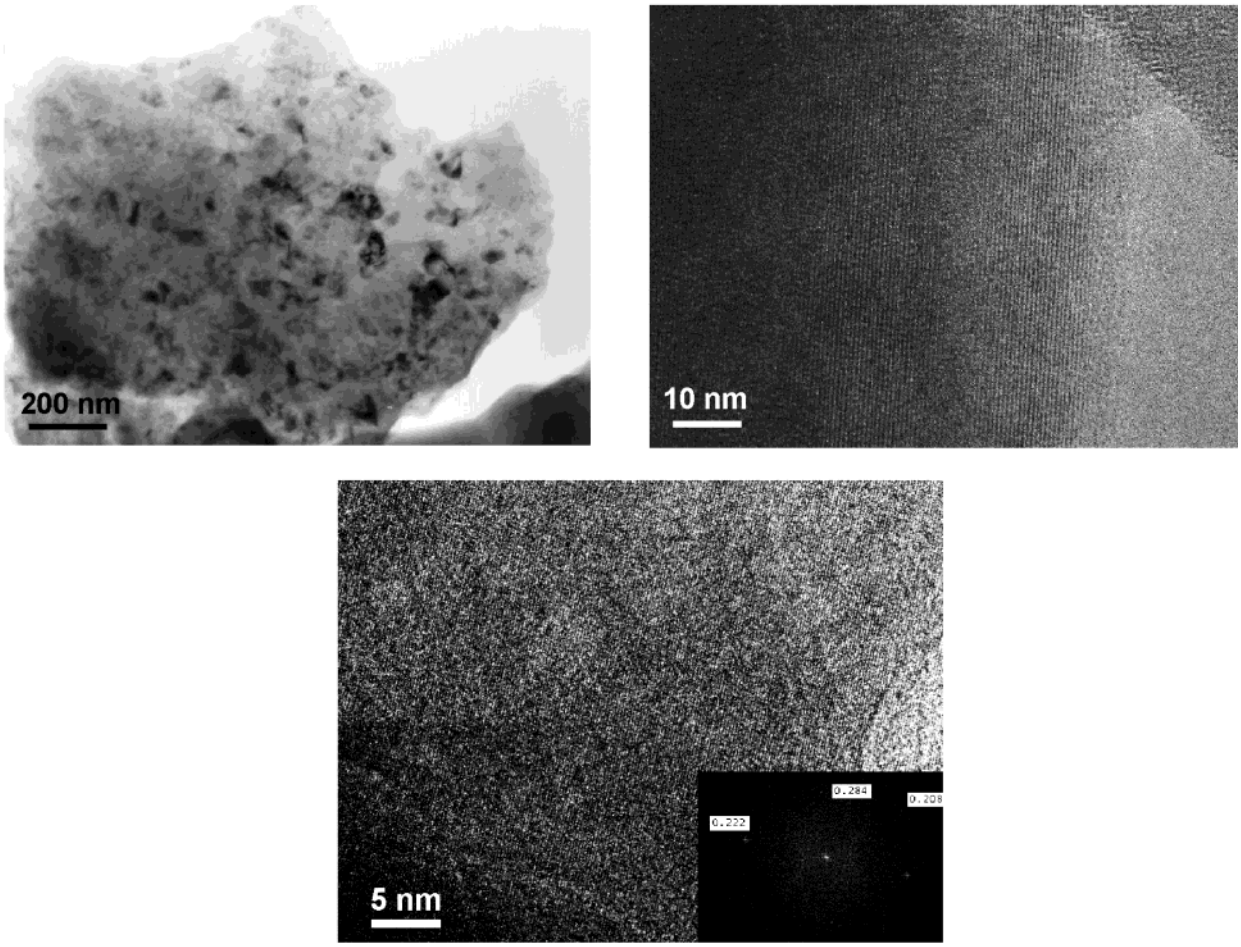

Figure 9. TEM images of cross sections of films prepared from (a) 33% MTMS in TEOS and 10 mol % CTAB, showing crystalline grains of 50−100 nm, and (b) 50% MTMS in TEOS and a CTAB concentration of 10 mol %. The interplanar distance is 3.11 Å. (c) Pure TEOS and a F127 concentration of 0.5 mol %. The inset gives the Fourier transform of the image, showing interplanar distances of 2.08, 2.22, and 2.84 Å.

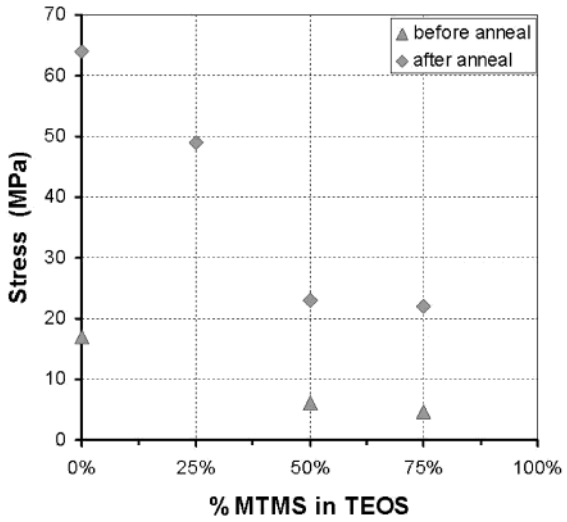

Figure 10. Stress, measured at 25 °C before and after annealing of the film at 400 °C in air, of films prepared from solutions containing various amount of MTMS in TEOS and 10 mol % CTAB as a surfactant.

ν is the Poisson ratio), h is the substrate thickness, R is the radius of curvature of the substrate induced by the film, and t is the film thickness.[32] The stress for films containing different amounts of MTMS is given in Figure 10. Stresses in the film are tensile. After spin coating of the film, the stress is relatively low, because the silica network is not fully cross-linked yet. During curing of the film, a stiff network is formed, leading to an increase of the stress. With an increasing content of methyl groups, the extent of cross-linking decreases, leading to a lowering of the elastic modulus of the film, which reduces the stress.

Determination of Young's Moduli. Low stiffness properties of novel low-*k* materials are one of the key factors limiting their introduction into ULSI technology. Some very different techniques can be used to measure the stiffness of low-*k* films. Most frequently, nanoindentation (NI) experiments are used to determine Young's modulus (E). However, for films as soft as low-*k* materials, this method must be performed very accurately to prevent an overestimation of the stiffness. In this study, NI results are compared to results obtained by two other techniques, SAWS and EP.

These three techniques are used to study a series of films prepared from solutions containing 50% MTMS in TEOS and varying amounts of CTAB (porosity). The results are summarized in Table 4. As expected, a higher porosity leads to a lower E. Furthermore, the data show that, when NI is correctly applied, all three techniques show similar results, although the methods use completely different physical models for calculation of E.

3.5. Back-End Integration: Etch Experiments. A first series of etch experiments has been performed to investigate the integration of this low-*k* material in the back-end processing of ICs (i.e., the deposition of dielectrics and metal interconnects). A solution containing 50% MTMS in TEOS and 13 mol % CTAB was spun onto a Si substrate with a stack of 50 nm Si_3N_4,

TABLE 4: Porosity and Young's Modulus (Measured by NI, EP, and SAWS) of Films Prepared from Solutions Containing 50% MTMS in TEOS and Varying Amounts of CTAB

		Youngs' modulus (MPa)		
CTAB amount	porosity	NI	SAWS	EP
7.6 mol %	48%	2.95	1.74	2.586
10 mol %	50%	1.27	1.46	1.512
12.5 mol %	56%	1.44	1.61	1.801
26.9 mol %	66%	0.41	0.31	0.472

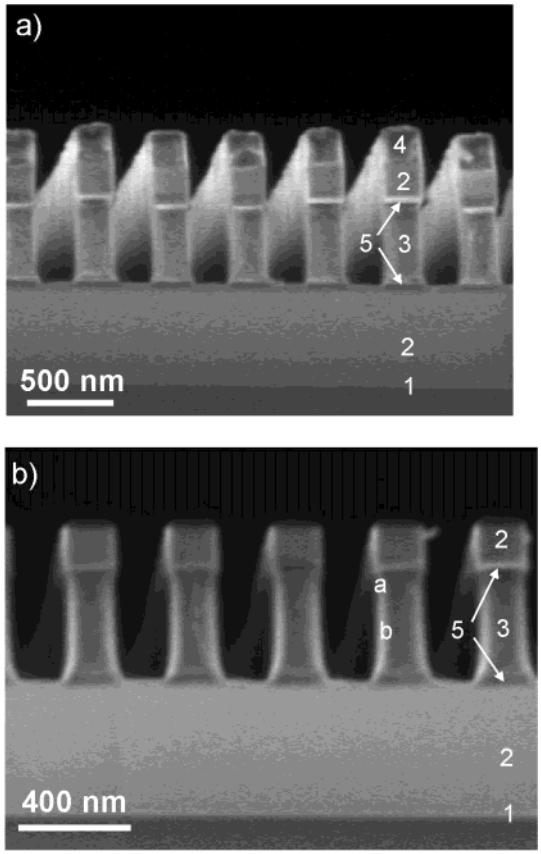

Figure 11. (a) Low-*k* stack after etching. (b) Same stack after resist stripping in O_2/N_2. Trenches are 200 nm wide. (1) Si_3N_4, (2) SiO_2, (3) low-*k*, (4) photoresist, and (5) SiC. The trenches show some undercutting (a) and bowing (b).

500 nm SiO_2, and 50 nm SiC. To promote adhesion, the SiC layer was treated in oxygen plasma prior to spin coating of the low-*k* dielectric. The resulting low-*k* film had a refractive index of 1.201. The estimated ϵ' for this film was 2.05. On top of the low-*k* film, 50 nm SiC, 150 nm SiO_2 (the "hard mask"), and 450 nm DUV (248 nm) photoresist was deposited. After lithographic patterning of the photoresist, the stack was etched. The hardmask was etched for 50 s in a $Ar/CF_4/CH_2F_2/O_2$ plasma, and the low-*k* film was subsequently etched during 20 s in a $Ar/CF_4/CH_2F_2/O_2$ plasma. The resulting etch pattern was well defined (see Figure 11a). To remove the photoresist after etching, the film was treated in N_2/O_2 plasma for 30 s. As shown in Figure 11b, this step also attacked the low-*k* film, resulting in some undercutting and bowing. Clearly, the resist stripping procedure needs to be optimized. Furthermore, it is known that an O_2 plasma is able to oxidize the methyl groups in porous organosilicates, leading to the formation of Si−OH groups, which will induce moisture uptake. It has been shown that this effect can be counteracted by treatment in hexamethyldisilazane vapor, which converts the Si−OH groups in S−CH_3 groups.[33]

4. Conclusions

A method to control the hydrophobicity and dielectric constant of mesoporous silica films for ultralow-*k* applications has been described. Cationic (CTAB) and nonionic (Brij76 and Pluronic F127) surfactants were used as sacrificial materials in (organo)silicate matrixes, prepared from tetraethoxysilane (TEOS) and methyl trimethoxysilane (MTMS). To optimize the film properties, several processing parameters were investigated.

Up to 90% of MTMS in TEOS can be incorporated in the mesoporous films. Films containing 50−60% MTMS in TEOS and CTAB as a surfactant are most attractive for low-*k* applications. FTIR shows that mesoporous films containing over 50% MTMS in TEOS do not show a Si−OH signal and are hydrophobic. Furthermore, CTAB is the surfactant for which the smallest pore sizes are obtained. However, films prepared from the nonionic surfactant Pluronic F127 showed to be more stable, probably caused by the increased wall thickness in these films. A disadvantage is the larger pore sizes.

The pore structure is reflected in the pore ordering as found in small angle XRD. This ordering decreases for increasing MTMS contents, and also, the *d* spacing decreases with increasing MTMS content. For slightly distorted rectangular or cubic pore structures, formed after annealing of the film, the interpore distance can be estimated from the *d* spacing and is close to $\sqrt{2}\, d_{(001)}$. This interpore distance can also be measured from TEM. Two indirect methods to measure pore sizes are EP and Kr adsorption. These techniques give comparable results; for a 50% porous film prepared from 50% MTMS in TEOS and CTAB as surfactant, a pore diameter of 2.8−3.0 nm is found. The pore size increases with increasing CTAB content, whereas the *d* spacing decreases with increasing amount of CTAB.

Surprisingly, high-resolution TEM shows a few percent crystallinity in the matrix of the mesoporous films, although it was not possible to deduce the mechanism of crystallization for mesoporous organosilica films. This, together with the results from ellipsometric porosimetry, at least strongly indicates that the matrix is quite dense, which is unique for the porous organosilicate low-*k* materials presently available. This, together with the small pores that can be obtained by using CTAB as a surfactant, will be an advantage for integration issues.

Acknowledgment. We thank R. Weemaes for performing the XRD, M. Kaiser for TEM, R. van de Ven and J. Dijk for preparing samples, S. Brongersma (IMEC, Leuven) for performing the nanoindentation experiments, and D. Schneider (Fraunhover Institute for Material and Beam Technology, Dresden) for SAWS.

References and Notes

(1) Zant, P. V. *Microchip Fabrication: A Practical Guide to Semiconductor Processing 4th ed.*; McGraw-Hill: New York, 2000; Vol. 1.

(2) *International Technology Road map for Semiconductors*; Semiconductor Industry Association: Austin, TX, 2001.

(3) Theis, T. N. *IBM J. Mater. Res. Develop.* **2000**, *44*, 379.

(4) Lin, X. W.; Pramanik, D. *Solid State Technol.* **2000**, *oct*, 63.

(5) Peters, L. *Semiconductor International*; http://www.einsite.net/semiconductor/index.asp?layout=article&articleId=CA169986&stt=001, Nov 1999.

(6) *International Technology Road map for Semiconductors*; Semiconductor Industry Association: Austin, TX, 1999.

(7) Miller, R. D. *International Sematech ultralow-k workshop*; San Francisco, 2002, Semiconductor Industry Association: Austin, TX.

(8) Atsushi, S.; Manabu, S.; Hisashi, N.; Michihiro, M.; Tatsusya, Y. *International Sematech ultralow-k workshop;* San Francisco, CA, 2002, Semiconductor Industry Association: Austin, TX.

(9) Golden, J. H.; Hawker, C. J.; Ho, P. S. http://www.jysong.idv.tw/cu/articles/cu0010.htm, 2001.
(10) Fan, H.; Brinker, C. J.; Ahlburn, B. T.; MacDougall, J. *International Sematech ultralow-k workshop;* San Francisco, CA, 2002, Semiconductor Industry Association: Austin, TX.
(11) Burkett, S.; Sims, S. D.; Mann, S. *Chem. Commun.* **1996**, 1367.
(12) Schneider, D.; Schwarz, T.; Scheibe, H.-J.; Panzer, M. *Thin Solid Films* **1997**, *295*, 107.
(13) Flannery, C. M.; Wittowski, T.; Jung, K.; Hillebrands, B.; Baklanov, M. R. *Appl. Phys. Lett.* **2002**, *80*, 4594.
(14) Mogilnikov, K. P.; Baklanov, M. R. *Electrochem. Sol. State Lett.* **2002**, *5*, F29.
(15) Aspnes, D. E. *Am. J. Phys.* **1982**, 704.
(16) Balkenende, A. R.; de Theije, F. K.; Kriege, J. C. *Adv. Mater*. **2003**, *15*, 140.
(17) Zhao, D.; Huo, Q.; Feng, J.; Chmelka, B. F.; Stucky, G. D. *J. Am. Chem. Soc.* **1998**, *120*, 6024.
(18) Huo, Q.; Margolese, D. I.; Ciesla, U.; Feng, P.; Gier, T. E.; Sieger, P.; Leon, R.; Petroff, P. M.; Schüth, F.; Stucky, G. D. *Nature* **1994**, *368*, 317.
(19) Huo, Q.; Margolese, D. I.; Ciesla, U.; Demuth, D. G.; Feng, P.; Gier, T. E.; Sieger, P.; Firouzi, A.; Chmelka, B. F.; Schüth, F.; Stucky, G. D. *Chem. Mater*. **1994**, *6*, 1176.
(20) Alonso, B.; Balkenende, A. R.; Albouy, P.-A.; Amenitsch, H.; Rager, M.-N.; Babonneau, F. *J. Sol-Gel Sci. Technol.* **2003**, *26*, 587.
(21) Jacobs, J. W. M.; Verhoeven, J. F. C. M. *J. Microscopy* **1986**, *143*, 103.
(22) Baklanov, M. R.; Mogilnikov, K. P. *Microelectron. Eng.* **2002**, *64*, 335.
(23) Takei, T.; Chikazawa, M. *J. Ceram. Soc. Jpn.* **1998**, *106*, 353.
(24) Gregg, S. J.; Sing, K. S. W. *Adsorption, Surface Area and Porosity*; Academic Press: London, 1967; Chapter 3.
(25) Bordiga, S.; Damin, A.; Bonino, F.; Zecchina, A.; Spano, G.; Rivetti, F.; Bolis, V.; Prestipino, C.; Lamberti, C. *J. Phys. Chem. B* **2002**, *106*, 9892.
(26) Nakano, T.; Tokunaga, K.; Ohta, T. *J. Eletrochem. Soc.* **1995**, *142*, 1303.
(27) Wang, C. Y.; Shen, Z. X.; Zheng, J. Z. *Appl. Spectrosc.* **2001**, *55*, 1347.
(28) Inagaki, S.; Guan, S.; Ohsuna, T.; Terasaki, O. *Nature* **2002**, *416*, 304.
(29) Davis, M. E. *Nature* **2002**, *417*, 813.
(30) Lu, Y.; Ganguli, R.; Drewien, C. A.; Anderson, M. T.; Brinker, C. J.; Gong, W.; Guo, Y.; Soyez, H.; Dunn, B.; Huang, M. H.; Zink, J. I. *Nature* **1997**, *389*, 364.
(31) Grosso, D.; Balkenende, A. R.; Albouy, P. A.; Lavergne, M.; Mazerolles, L.; Babonneau, F. *J. Mater. Chem.* **2000**, *10*, 2085.
(32) Stoney, G. *Proc. R. Soc. London Ser. A* **1909**, *82*, 172.
(33) Chang, T. C.; Mor, Y. S.; Liu, P. T.; Tsai, T. M.; Chen, C. W.; Mei, Y. J.; Sze, S. M. *J. Electrochem. Soc.* **2002**, *149*, F81.